Journal of Zhejiang University-SCIENCE C (Computers & Electronics)
ISSN 1869-1951 (Print); ISSN 1869-196X (Online)
www.zju.edu.cn/jzus; www.springerlink.com
E-mail: jzus@zju.edu.cn

Motion synchronization of dual-cylinder pneumatic servo systems with integration of adaptive robust control and cross-coupling approach*

De-yuan MENG[†1,2], Guo-liang TAO[†2], Ai-min LI[1], Wei LI[1]

([1]*School of Mechatronic Engineering, China University of Mining and Technology, Xuzhou 221116, China*)

([2]*State Key Laboratory of Fluid Power Transmission and Control, Zhejiang University, Hangzhou 310027, China*)

[†]E-mail: tinydream@zju.edu.cn; gltao@zju.edu.cn

Received Dec. 11, 2013; Revision accepted Apr. 13, 2014; Crosschecked July 16, 2014

Abstract: We investigate motion synchronization of dual-cylinder pneumatic servo systems and develop an adaptive robust synchronization controller. The proposed controller incorporates the cross-coupling technology into the integrated direct/indirect adaptive robust control (DIARC) architecture by feeding back the coupled position errors, which are formed by the trajectory tracking errors of two cylinders and the synchronization error between them. The controller employs an online recursive least squares estimation algorithm to obtain accurate estimates of model parameters for reducing the extent of parametric uncertainties, and uses a robust control law to attenuate the effects of parameter estimation errors, unmodeled dynamics, and disturbances. Therefore, asymptotic convergence to zero of both trajectory tracking and synchronization errors can be guaranteed. Experimental results verify the effectiveness of the proposed controller.

Key words: Motion synchronization, Pneumatic servo system, Cross-coupling, Adaptive robust control
doi:10.1631/jzus.C1300360 **Document code:** A **CLC number:** TP202; TH138

1 Introduction

The problem of synchronizing two pneumatic cylinders arises in pneumatic operated applications such as lifting equipment, medical instruments, and semiconductor processing devices. Traditional motion synchronization among multiple pneumatic actuators has been implemented by linkage mechanisms in open-loop operations. However, mechanical linkages are not adequate to achieve high-performance motion synchronization in the presence of load variation, model uncertainties, and external disturbances. In addition, mechanical synchronization has limitation to the operation range of the equipment. Thus, feedback control methods are necessary for high precision synchronized motion control of multiple pneumatic actuators.

Several synchronization approaches were considered in Jang *et al.* (2004), Shibata *et al.* (2006), and Zhu *et al.* (2009). In these studies, similar control architectures with an individual controller for each of the pneumatic cylinders and a synchronization controller were proposed. Each pneumatic cylinder was controlled separately by its own individual controller to track its desired trajectory, while the synchronization errors amongst cylinders were fed to the synchronization controller and the output of which was added to cylinder controllers for reducing the synchronization errors. This method was also applied to the synchronization control of two hydraulic cylinders (Chen, 2007; Chen *et al.*, 2008) and linear motors (Hsieh *et al.*, 2007). However, the issue of how to design a control algorithm that will explicitly achieve a bounded synchronization error is yet to be resolved.

* Project supported by the Fundamental Research Funds for the Central Universities, China (No. 2014QNA40) and the Natural Science Foundation of Jiangsu Province, China (No. BK20140188)

Furthermore, since the precision motion trajectory tracking control of a single pneumatic cylinder is still a big challenge, the achievable motion synchronization performance is not satisfactory.

During the past decade, the cross-coupling method (Koren, 1980) was employed to design the controllers for position synchronization of multiple motion axes (Sun, 2003; Xiao *et al.*, 2005; Xiao and Zhu, 2006; Sun *et al.*, 2007). For example, in Sun (2003), the position synchronization error of each axis was coupled with the position error to form a coupled position error. An adaptive coupling controller with feedback of this coupled position error was proposed and proven to guarantee asymptotic convergence to zero of both position and synchronization errors. The cross-coupling concept has also been widely used in robotics (Sun and Mills, 2002), control of parallel manipulators (Su *et al.*, 2006; Sun *et al.*, 2006), formation control of multiple mobile robots (Sun *et al.*, 2009), and synchronized trajectory tracking control of multiple 3-DOF (degree of freedom) experimental helicopters (Shan *et al.*, 2005).

In Meng *et al.* (2013), an integrated direct/indirect adaptive robust controller (DIARC) was developed for the motion trajectory tracking control of a pneumatic cylinder driven by a proportional directional control valve. The controller employs a physical model based indirect-type parameter estimation to obtain reliable estimates of unknown model parameters, and uses a robust control method with fast dynamic compensation type model compensation to attenuate the effects of parameter estimation errors, unmodeled dynamics, and disturbances. Extensive experimental results were presented to illustrate the excellent achievable performance of the proposed controller and performance robustness to load variation and sudden disturbance.

In this paper, the synchronization of two pneumatic cylinders that are not mechanically connected is considered (Fig. 1). To achieve a high performance

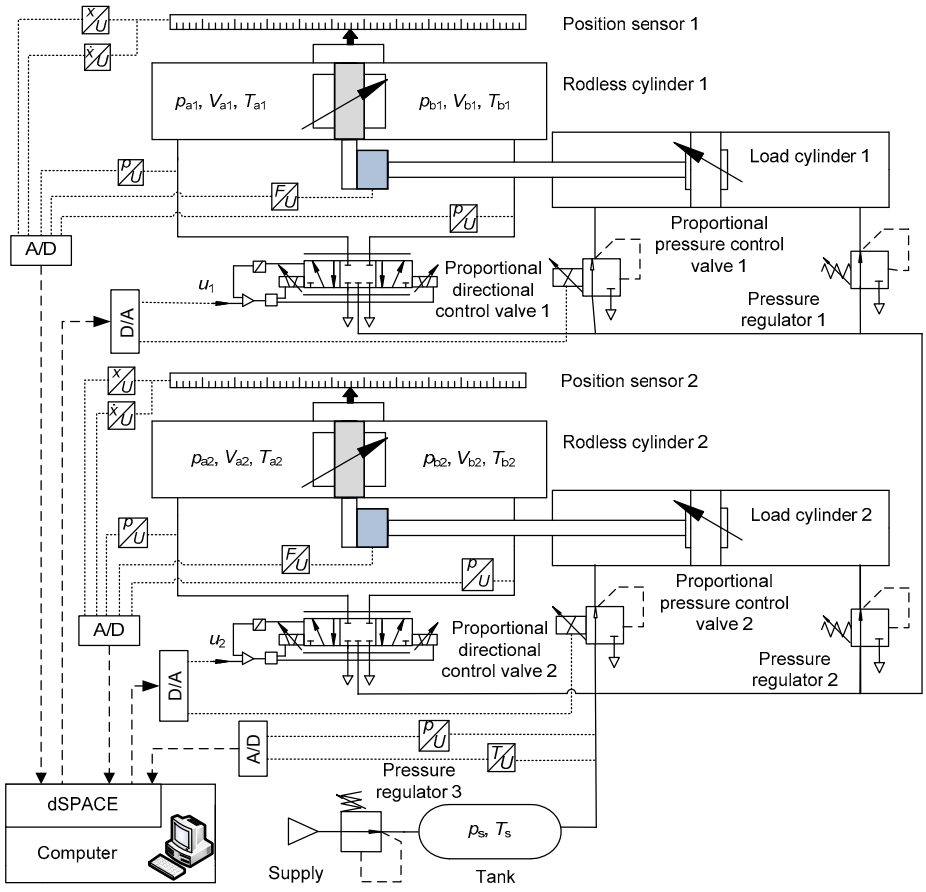

Fig. 1 Schematic of the dual-cylinder pneumatic servo system

synchronized motion trajectory tracking control of dual-cylinder pneumatic servo systems, an adaptive robust synchronization control strategy which incorporates the cross-coupling concept into the DIARC architecture is proposed.

2 Dynamic models

As shown in Fig. 1, each rodless pneumatic cylinder of the dual-cylinder pneumatic servo system is controlled by a proportional directional control valve (FESTO MPYE-5-1/8-HF-010B). The motion of the piston-load assemblies of the two cylinders can be described by

$$\boldsymbol{M}\ddot{\boldsymbol{x}} = A\boldsymbol{p}_{\mathrm{L}} - \boldsymbol{b}\dot{\boldsymbol{x}} - \boldsymbol{F}_{\mathrm{C}}(\dot{\boldsymbol{x}}) - \boldsymbol{F}_{\mathrm{L}} + \boldsymbol{f}, \tag{1}$$

where $\boldsymbol{M}$=diag$\{M_1, M_2\}$ and $\boldsymbol{b}$=diag$\{b_1, b_2\}$ are the 2×2 diagonal inertia and viscous friction coefficient matrices, respectively, M_1 and M_2 are the lumped masses of the piston-load assemblies of the two cylinders, $\boldsymbol{x}=[x_1, x_2]^{\mathrm{T}}$, $\dot{\boldsymbol{x}}=[\dot{x}_1, \dot{x}_2]^{\mathrm{T}}$, and $\ddot{\boldsymbol{x}}=[\ddot{x}_1, \ddot{x}_2]^{\mathrm{T}}$ are the 2×1 vectors of piston position, velocity, and acceleration, respectively, A is the piston effective area, $\boldsymbol{p}_{\mathrm{L}}=[p_{\mathrm{L1}}, p_{\mathrm{L2}}]^{\mathrm{T}}$ is the 2×1 vector of pressure differential across the piston, in which $p_{\mathrm{L1}}=p_{\mathrm{a1}}-p_{\mathrm{b1}}$, $p_{\mathrm{L2}}=p_{\mathrm{a2}}-p_{\mathrm{b2}}$, p_{a1}, p_{a2}, p_{b1}, and p_{b2} are the absolute pressures of the left and right chambers of two cylinders, respectively, $\boldsymbol{F}_{\mathrm{C}}(\dot{\boldsymbol{x}})$ is the 2×1 vector of Coulomb friction, modeled by $\boldsymbol{F}_{\mathrm{C}}(\dot{\boldsymbol{x}})=\boldsymbol{A}_{\mathrm{f}}\boldsymbol{S}_{\mathrm{f}}(\dot{\boldsymbol{x}})$, where $\boldsymbol{A}_{\mathrm{f}}$=diag$\{A_{\mathrm{f1}}, A_{\mathrm{f2}}\}$ is the 2×2 unknown Coulomb friction coefficient matrix and $\boldsymbol{S}_{\mathrm{f}}(\dot{\boldsymbol{x}})=[S_{\mathrm{f1}}(\dot{x}_1), S_{\mathrm{f2}}(\dot{x}_2)]^{\mathrm{T}}$ is a known 2×1 vector of smooth function used to approximate the traditional discontinuous sign function $\mathrm{sgn}(\dot{\boldsymbol{x}})$ used in the traditional Coulomb friction modeling for effective friction compensation in complementation (Meng *et al.*, 2013), $\boldsymbol{F}_{\mathrm{L}}=[F_{\mathrm{L1}}, F_{\mathrm{L2}}]^{\mathrm{T}}$ is the 2×1 vector of external load force, and $\boldsymbol{f}$ is the 2×1 vector of lumped modeling error including external disturbances and terms like the unmodeled friction forces and other uncertainties. Let $\boldsymbol{f}_{\mathrm{n}}=[f_{\mathrm{n1}}, f_{\mathrm{n2}}]^{\mathrm{T}}$ be the nominal value of $\boldsymbol{f}$ and $\tilde{\boldsymbol{f}}_0=\boldsymbol{f}-\boldsymbol{f}_{\mathrm{n}}$ the time-varying portion of $\boldsymbol{f}$. The motion of the piston-load assemblies of the two cylinders can be rewritten as

$$\boldsymbol{M}\ddot{\boldsymbol{x}} = A\boldsymbol{p}_{\mathrm{L}} - \boldsymbol{b}\dot{\boldsymbol{x}} - \boldsymbol{A}_{\mathrm{f}}\boldsymbol{S}_{\mathrm{f}}(\dot{\boldsymbol{x}}) - \boldsymbol{F}_{\mathrm{L}} + \boldsymbol{f}_{\mathrm{n}} + \tilde{\boldsymbol{f}}_0. \tag{2}$$

Define the unknown parameter set $\boldsymbol{\theta}_{\mathrm{l}}=[\theta_{11}, \theta_{12}, \theta_{13}, \theta_{14}, \theta_{15}, \theta_{16}]^{\mathrm{T}}$ as $\theta_{11}=b_1$, $\theta_{12}=A_{\mathrm{f1}}$, $\theta_{13}=-F_{\mathrm{L1}}+f_{\mathrm{n1}}$, $\theta_{14}=b_2$, $\theta_{15}=A_{\mathrm{f2}}$, $\theta_{16}=-F_{\mathrm{L2}}+f_{\mathrm{n2}}$. Eq. (2) can be further rewritten as

$$\boldsymbol{M}\ddot{\boldsymbol{x}} = A\boldsymbol{p}_{\mathrm{L}} + \boldsymbol{\varphi}_{\mathrm{l}}^{\mathrm{T}}\boldsymbol{\theta}_{\mathrm{l}} + \tilde{\boldsymbol{f}}_0, \tag{3}$$

where $\boldsymbol{\varphi}_{\mathrm{l}}^{\mathrm{T}}=\begin{bmatrix} \dot{x}_1 & S_{\mathrm{f1}}(\dot{x}_1) & 1 & 0 & 0 & 0 \\ 0 & 0 & 0 & \dot{x}_2 & S_{\mathrm{f2}}(\dot{x}_2) & 1 \end{bmatrix}$ is a 6×2 matrix of known functions, commonly referred to as the regressor.

The differential equation that describes the pressure build-up in two cylinders is given by

$$\dot{\boldsymbol{p}}_{\mathrm{L}} = \boldsymbol{q}_{\mathrm{L}} + \boldsymbol{F}_{\mathrm{p}} + \boldsymbol{d}, \tag{4}$$

where

$$\boldsymbol{q}_{\mathrm{L}}=\begin{bmatrix} q_{\mathrm{L1}} \\ q_{\mathrm{L2}} \end{bmatrix}=\begin{bmatrix} \dfrac{\gamma R}{V_{\mathrm{a1}}}(\dot{m}_{\mathrm{ain1}}T_{\mathrm{s}}-\dot{m}_{\mathrm{aout1}}T_{\mathrm{a1}})-\dfrac{\gamma R}{V_{\mathrm{b1}}}(\dot{m}_{\mathrm{bin1}}T_{\mathrm{s}}-\dot{m}_{\mathrm{bout1}}T_{\mathrm{b1}}) \\ \dfrac{\gamma R}{V_{\mathrm{a2}}}(\dot{m}_{\mathrm{ain2}}T_{\mathrm{s}}-\dot{m}_{\mathrm{aout2}}T_{\mathrm{a2}})-\dfrac{\gamma R}{V_{\mathrm{b2}}}(\dot{m}_{\mathrm{bin2}}T_{\mathrm{s}}-\dot{m}_{\mathrm{bout2}}T_{\mathrm{b2}}) \end{bmatrix}$$

and

$$\boldsymbol{F}_{\mathrm{p}}=\begin{bmatrix} -\dfrac{\gamma A}{V_{\mathrm{a1}}}\dot{x}_1 p_{\mathrm{a1}}-\dfrac{\gamma A}{V_{\mathrm{b1}}}\dot{x}_1 p_{\mathrm{b1}}+\dfrac{\gamma-1}{V_{\mathrm{a1}}}\dot{Q}_{\mathrm{a1}}-\dfrac{\gamma-1}{V_{\mathrm{b1}}}\dot{Q}_{\mathrm{b1}} \\ -\dfrac{\gamma A}{V_{\mathrm{a2}}}\dot{x}_2 p_{\mathrm{a2}}-\dfrac{\gamma A}{V_{\mathrm{b2}}}\dot{x}_2 p_{\mathrm{b2}}+\dfrac{\gamma-1}{V_{\mathrm{a2}}}\dot{Q}_{\mathrm{a2}}-\dfrac{\gamma-1}{V_{\mathrm{b2}}}\dot{Q}_{\mathrm{b2}} \end{bmatrix}$$

are two 2×1 vectors of known functions, in which γ is the ratio of specific heats, R is the gas constant, V_{a1}, V_{a2}, V_{b1}, and V_{b2} are the volumes of the left and right chambers of two cylinders, respectively, T_{a1}, T_{a2}, T_{b1}, and T_{b2} are the gas temperatures inside the left and right chambers of two cylinders, respectively, T_{s} is the ambient temperature, $\dot{m}_{\mathrm{ain1}}$, $\dot{m}_{\mathrm{ain2}}$, $\dot{m}_{\mathrm{bin1}}$, and $\dot{m}_{\mathrm{bin2}}$ are the mass flows entering the left and right chambers of two cylinders, respectively, $\dot{m}_{\mathrm{aout1}}$, $\dot{m}_{\mathrm{aout2}}$, $\dot{m}_{\mathrm{bout1}}$, and $\dot{m}_{\mathrm{bout2}}$ are the mass flows leaving the left and right chambers of two cylinders, respectively, $\dot{Q}_{\mathrm{a1}}$, $\dot{Q}_{\mathrm{a2}}$, $\dot{Q}_{\mathrm{b1}}$, and $\dot{Q}_{\mathrm{b2}}$ represent the heat transfer between the air in the cylinder chambers and the inside of the barrel, and $\boldsymbol{d}$ is the 2×1 vector of lumped unknown nonlinear functions due to external disturbances and modeling errors. Let $\boldsymbol{d}_{\mathrm{n}}=[d_{\mathrm{n1}}, d_{\mathrm{n2}}]^{\mathrm{T}}$ be

the nominal value of $\boldsymbol{d}$ and $\tilde{\boldsymbol{d}}_0=\boldsymbol{d}-\boldsymbol{d}_\mathrm{n}$ the time-varying portion of $\boldsymbol{d}$. Moreover, define the unknown parameter set $\boldsymbol{\theta}_2=[\theta_{21}, \theta_{22}]^\mathrm{T}$ as $\theta_{21}=d_{\mathrm{n}1}$, $\theta_{22}=d_{\mathrm{n}2}$. Eq. (4) can be rewritten as

$$\dot{\boldsymbol{p}}_\mathrm{L}=\boldsymbol{q}_\mathrm{L}+\boldsymbol{F}_\mathrm{p}+\boldsymbol{\varphi}_2^\mathrm{T}\boldsymbol{\theta}_2+\tilde{\boldsymbol{d}}_0, \tag{5}$$

where $\boldsymbol{\varphi}_2^\mathrm{T}=\begin{bmatrix}1 & 0\\ 0 & 1\end{bmatrix}$ is the 2×2 regressor matrix.

According to Carneiro and de Almeida (2006) and Meng *et al.* (2011), the gas temperatures inside the cylinder chambers can be estimated by

$$\begin{cases}T_{\mathrm{a}1}=T_\mathrm{s}\left(\dfrac{p_{\mathrm{a}1}}{0.8077p_\mathrm{s}}\right)^{\frac{n_\mathrm{p}-1}{n_\mathrm{p}}}, \ T_{\mathrm{a}2}=T_\mathrm{s}\left(\dfrac{p_{\mathrm{a}2}}{0.8077p_\mathrm{s}}\right)^{\frac{n_\mathrm{p}-1}{n_\mathrm{p}}},\\ T_{\mathrm{b}1}=T_\mathrm{s}\left(\dfrac{p_{\mathrm{b}1}}{0.8077p_\mathrm{s}}\right)^{\frac{n_\mathrm{p}-1}{n_\mathrm{p}}}, \ T_{\mathrm{b}2}=T_\mathrm{s}\left(\dfrac{p_{\mathrm{b}2}}{0.8077p_\mathrm{s}}\right)^{\frac{n_\mathrm{p}-1}{n_\mathrm{p}}},\end{cases} \tag{6}$$

where p_s is the supply pressure and n_p is the polytropic index with a value of 1.35. Choosing the middle of the stroke as the origin of piston displacement, the volumes of the left and right chambers of two cylinders can be expressed as

$$\begin{cases}V_{\mathrm{a}1}=V_{\mathrm{a}10}+A(L/2+x_1),\\ V_{\mathrm{a}2}=V_{\mathrm{a}20}+A(L/2+x_2),\\ V_{\mathrm{b}1}=V_{\mathrm{b}10}+A(L/2-x_1),\\ V_{\mathrm{b}2}=V_{\mathrm{b}20}+A(L/2-x_2),\end{cases} \tag{7}$$

where $V_{\mathrm{a}10}$, $V_{\mathrm{a}20}$, $V_{\mathrm{b}10}$, and $V_{\mathrm{b}20}$ are the dead volumes of two cylinders at the beginning and the end of the stroke, including fittings and lines, and L is the piston stroke. The heat transfer between the air in the cylinder chambers and the inside of the barrel can be determined by

$$\begin{cases}\dot{Q}_{\mathrm{a}1}=hS_{\mathrm{a}1}(x_1)\cdot(T_\mathrm{s}-T_{\mathrm{a}1}),\\ \dot{Q}_{\mathrm{b}1}=hS_{\mathrm{b}1}(x_1)\cdot(T_\mathrm{s}-T_{\mathrm{b}1}),\\ \dot{Q}_{\mathrm{a}2}=hS_{\mathrm{a}2}(x_2)\cdot(T_\mathrm{s}-T_{\mathrm{a}2}),\\ \dot{Q}_{\mathrm{b}2}=hS_{\mathrm{b}2}(x_2)\cdot(T_\mathrm{s}-T_{\mathrm{b}2}),\end{cases} \tag{8}$$

where h is the heat transfer coefficient, and $S_{\mathrm{a}1}(x_1)$, $S_{\mathrm{b}1}(x_1)$, $S_{\mathrm{a}2}(x_2)$, and $S_{\mathrm{b}2}(x_2)$ are the heat transfer surface areas, which can be calculated by

$$\begin{cases}S_{\mathrm{a}1}(x_1)=2A+\pi D(L/2+x_1),\\ S_{\mathrm{a}2}(x_2)=2A+\pi D(L/2+x_2),\\ S_{\mathrm{b}1}(x_1)=2A+\pi D(L/2-x_1),\\ S_{\mathrm{b}2}(x_2)=2A+\pi D(L/2-x_2),\end{cases} \tag{9}$$

where D is the diameter of the piston.

According to Meng *et al.* (2011; 2013), the mass flows entering or leaving the cylinder chambers can be described by

$$\dot{m}_i=A_i(u_i)K_\mathrm{q}(p_\mathrm{u},p_\mathrm{d},T_\mathrm{u})=$$
$$\begin{cases}A_i(u_i)C_\mathrm{d}C_1\dfrac{p_\mathrm{u}}{\sqrt{T_\mathrm{u}}}, & \dfrac{p_\mathrm{d}}{p_\mathrm{u}}\le p_\mathrm{r},\\ A_i(u_i)C_\mathrm{d}C_1\dfrac{p_\mathrm{u}}{\sqrt{T_\mathrm{u}}}\sqrt{1-\left(\dfrac{\frac{p_\mathrm{d}}{p_\mathrm{u}}-p_\mathrm{r}}{1-p_\mathrm{r}}\right)^2}, & p_\mathrm{r}<\dfrac{p_\mathrm{d}}{p_\mathrm{u}}<\lambda,\\ A_i(u_i)C_\mathrm{d}C_1\dfrac{p_\mathrm{u}}{\sqrt{T_\mathrm{u}}}\left(\dfrac{1-\frac{p_\mathrm{d}}{p_\mathrm{u}}}{1-\lambda}\right)\sqrt{1-\left(\dfrac{\lambda-p_\mathrm{r}}{1-p_\mathrm{r}}\right)^2}, & \lambda\le\dfrac{p_\mathrm{d}}{p_\mathrm{u}}\le 1,\end{cases} \tag{10}$$

where i=1, 2 is the control valve's index, $\dot{m}_i$ is the mass flow rate, $A_i(u_i)$ is the effective valve orifice area, u_i is the control valve's control input, C_d is the discharge coefficient, C_1 is a constant with a value of 0.0404, p_u and p_d are the upstream pressure and the downstream pressure, respectively, T_u is the upstream temperature of air, p_r is the critical pressure ratio, and λ is the minimum pressure ratio to have a laminar flow, which takes a value close to 1. Fig. 2 shows the relationship between input signal u_i and orifice area (input and exhaust paths) $A_i(u_i)$, i=1, 2.

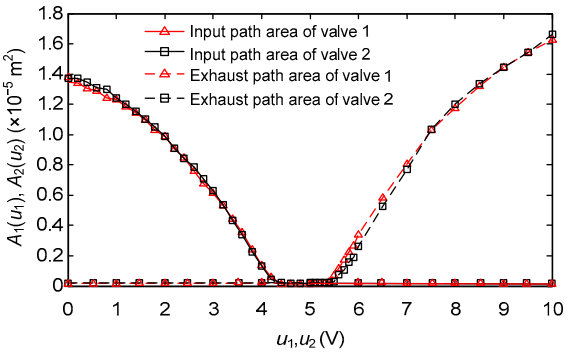

Fig. 2 Input and exhaust path valve areas vs. input signal

Assumption 1 The extent of parametric uncertainties and uncertain nonlinearities is known; i.e.,

$$\begin{cases} \boldsymbol{\theta}_i \in \Omega_{\boldsymbol{\theta}_i} \triangleq \{\boldsymbol{\theta}_i : \boldsymbol{\theta}_{i\min} \le \boldsymbol{\theta}_i \le \boldsymbol{\theta}_{i\max}\},\ i=1,2, \\ \tilde{\boldsymbol{f}}_0 \in \Omega_{\tilde{f}_0} \triangleq \{\tilde{\boldsymbol{f}}_0 : \left\|\tilde{\boldsymbol{f}}_0\right\| \le f_{\max}\}, \\ \tilde{\boldsymbol{d}}_0 \in \Omega_{\tilde{d}_0} \triangleq \{\tilde{\boldsymbol{d}}_0 : \left\|\tilde{\boldsymbol{d}}_0\right\| \le d_{\max}\}, \end{cases} \tag{11}$$

where $\boldsymbol{\theta}_{1\min}=[\theta_{11\min},\ \theta_{12\min},\ \theta_{13\min},\ \theta_{14\min},\ \theta_{15\min},\ \theta_{16\min}]^{\mathrm{T}}$ and $\boldsymbol{\theta}_{2\min}=[\theta_{21\min},\ \theta_{22\min}]^{\mathrm{T}}$ are the minimum parameter vectors, $\boldsymbol{\theta}_{1\max}=[\theta_{11\max}, \theta_{12\max}, \theta_{13\max}, \theta_{14\max},\ \theta_{15\max},\ \theta_{16\max}]^{\mathrm{T}}$ and $\boldsymbol{\theta}_{2\max}=[\theta_{21\max},\ \theta_{22\max}]^{\mathrm{T}}$ are the maximum parameter vectors, and $f_{\max}$ and $d_{\max}$ are known positive scalars.

3 Controller design

In this section, an adaptive robust synchronization controller for multi-cylinder pneumatic servo system is developed by incorporating the cross-coupling technology into the DIARC architecture. The proposed controller comprises an online recursive least squares estimation (RLSE) algorithm and a robust control law. The former is employed to obtain accurate estimates of model parameters for reducing the extent of parametric uncertainties, while the latter is utilized to attenuate the effects of parameter estimation errors, unmodeled dynamics and disturbances. The robust control law and the parameter adaption algorithm can be designed separately with the use of projection mapping. Since the system model uncertainties are unmatched, the recursive backstepping technology is adopted to design the robust control law.

3.1 Robust control law

Define the motion trajectory tracking error vector of the two cylinders as

$$\boldsymbol{e}=\begin{bmatrix} e_1 \\ e_2 \end{bmatrix}=\begin{bmatrix} x_1-x_{\mathrm{d}} \\ x_2-x_{\mathrm{d}} \end{bmatrix}=\boldsymbol{x}-\boldsymbol{x}_{\mathrm{d}}, \tag{12}$$

where $\boldsymbol{x}_{\mathrm{d}}=[x_{\mathrm{d}}, x_{\mathrm{d}}]^{\mathrm{T}}$ is a 2×1 vector of the desired motion trajectory. Obviously, the motion synchronization goal will be achieved if $e_1=e_2$. Thus, we define the position synchronization error vector of the two cylinders in the following way:

$$\boldsymbol{\varsigma}=\begin{bmatrix} \varsigma_1 \\ \varsigma_2 \end{bmatrix}=\begin{bmatrix} e_1-e_2 \\ e_2-e_1 \end{bmatrix}=\boldsymbol{T}\boldsymbol{e}, \tag{13}$$

where $\boldsymbol{T}=\begin{bmatrix} 1 & -1 \\ -1 & 1 \end{bmatrix}$ is the 2×2 synchronization transformation matrix. According to the concept of cross-coupling approach, a coupled position error vector $\boldsymbol{E}=[E_1, E_2]^{\mathrm{T}}$ that contains both the motion trajectory tracking error vector $\boldsymbol{e}$ and the synchronization error $\boldsymbol{\varsigma}$ is introduced:

$$\boldsymbol{E}=\boldsymbol{e}+\boldsymbol{\beta}\boldsymbol{T}^{\mathrm{T}}\int_0^t \boldsymbol{\varsigma}\mathrm{d}\omega, \tag{14}$$

where $\boldsymbol{\beta}=\mathrm{diag}\{\beta, \beta\}$ is a positive-definite coupling gain matrix, which determines the weight of the synchronization error $\boldsymbol{\varsigma}$ in the coupled position error $\boldsymbol{E}$.

The recursive backstepping technology is adopted, and the following steps will be taken to synthesize a control input vector $\boldsymbol{u}=[u_1, u_2]^{\mathrm{T}}$ for two control valves such that $\boldsymbol{x}$ tracks the desired trajectory $\boldsymbol{x}_{\mathrm{d}}$ while achieving precise motion synchronization of the two cylinders.

3.1.1 Step 1

Define a switch-function-like quantity as

$$\boldsymbol{r}=\dot{\boldsymbol{E}}+\boldsymbol{\Lambda}\boldsymbol{E}, \tag{15}$$

where $\boldsymbol{\Lambda}=\mathrm{diag}\{\Lambda, \Lambda\}$ is a positive-definite feedback gain matrix. Differentiating $\boldsymbol{r}$ with respect to time leads to

$$\dot{\boldsymbol{r}}=\ddot{\boldsymbol{e}}+\boldsymbol{\beta}\boldsymbol{T}^{\mathrm{T}}\dot{\boldsymbol{\varsigma}}+\boldsymbol{\Lambda}\dot{\boldsymbol{e}}+\boldsymbol{\Lambda}\boldsymbol{\beta}\boldsymbol{T}^{\mathrm{T}}\boldsymbol{\varsigma}. \tag{16}$$

Define a positive semi-definite function

$$\begin{aligned} V_1=&\frac{1}{2}\boldsymbol{r}^{\mathrm{T}}\boldsymbol{M}\boldsymbol{r}+\frac{1}{2}\boldsymbol{\varsigma}^{\mathrm{T}}\boldsymbol{K}_{\boldsymbol{\varsigma}}\boldsymbol{\varsigma} \\ &+\frac{1}{2}\left(\int_0^t \boldsymbol{T}^{\mathrm{T}}\boldsymbol{\varsigma}\mathrm{d}\omega\right)^{\mathrm{T}}\boldsymbol{\beta}\boldsymbol{\Lambda}\boldsymbol{K}_{\boldsymbol{\varsigma}}\left(\int_0^t \boldsymbol{T}^{\mathrm{T}}\boldsymbol{\varsigma}\mathrm{d}\omega\right), \end{aligned} \tag{17}$$

where $\boldsymbol{K}_{\varsigma}=\mathrm{diag}\{K_{\varsigma}, K_{\varsigma}\}$ is a positive-definite diagonal matrix. Differentiating V_1 and noting Eqs. (3) and (16), one obtains

$$\dot{V}_1 = \boldsymbol{r}^{\mathrm{T}}[A\boldsymbol{p}_{\mathrm{L}} + \boldsymbol{\varphi}_1^{\mathrm{T}}\boldsymbol{\theta}_1 + \tilde{\boldsymbol{f}}_0 - \boldsymbol{M}\ddot{\boldsymbol{x}}_{\mathrm{d}} + \boldsymbol{M}\boldsymbol{\beta}\boldsymbol{T}^{\mathrm{T}}\dot{\boldsymbol{\varsigma}} + \boldsymbol{M}\boldsymbol{\Lambda}\dot{\boldsymbol{E}}] + \boldsymbol{\varsigma}^{\mathrm{T}}\boldsymbol{K}_{\boldsymbol{\varsigma}}\dot{\boldsymbol{\varsigma}} + \left(\int_0^t \boldsymbol{T}^{\mathrm{T}}\boldsymbol{\varsigma}\mathrm{d}\omega\right)^{\mathrm{T}} \boldsymbol{\beta}\boldsymbol{\Lambda}\boldsymbol{K}_{\boldsymbol{\varsigma}}\boldsymbol{T}^{\mathrm{T}}\boldsymbol{\varsigma}. \tag{18}$$

Considering $\boldsymbol{p}_{\mathrm{L}}$ as the virtual control input, the following control law $\boldsymbol{p}_{\mathrm{Ld}}$ for $\boldsymbol{p}_{\mathrm{L}}$ is proposed:

$$\boldsymbol{p}_{\mathrm{Ld}} = \boldsymbol{p}_{\mathrm{Lda1}} + \boldsymbol{p}_{\mathrm{Lda2}} + \boldsymbol{p}_{\mathrm{Lds1}} + \boldsymbol{p}_{\mathrm{Lds2}}, \tag{19}$$

where

$$\boldsymbol{p}_{\mathrm{Lda1}} = \frac{1}{A}[-\boldsymbol{\varphi}_1^{\mathrm{T}}\hat{\boldsymbol{\theta}}_1 + \boldsymbol{M}(\ddot{\boldsymbol{x}}_{\mathrm{d}} - \boldsymbol{\beta}\boldsymbol{T}^{\mathrm{T}}\dot{\boldsymbol{\varsigma}} - \boldsymbol{\Lambda}\dot{\boldsymbol{E}}) - \boldsymbol{K}_{\boldsymbol{\varsigma}}\boldsymbol{T}^{\mathrm{T}}\boldsymbol{\varsigma}],$$

$$\boldsymbol{p}_{\mathrm{Lds1}} = -\boldsymbol{K}_{\mathrm{p}}\boldsymbol{r} / A.$$

$\boldsymbol{p}_{\mathrm{Lda1}}$ is the usual model compensation with the physical parameter estimate $\hat{\boldsymbol{\theta}}_1$ updated using an online adaption algorithm to be detailed in Section 3.2, $\boldsymbol{p}_{\mathrm{Lda2}}$ is a fast dynamic compensation type model compensation term discussed later in this section, $\boldsymbol{p}_{\mathrm{Lds1}}$ is a negative feedback of $\boldsymbol{r}$ to stabilize the nominal system, in which $\boldsymbol{K}_{\mathrm{p}}$=diag{$K_{\mathrm{p1}}$, K_{p2}} is a positive-definite diagonal control gain matrix, and $\boldsymbol{p}_{\mathrm{Lds2}}$ is a robust feedback term to be synthesized later so that some guaranteed robust performance can be achieved in spite of various model uncertainties. The last term in $\boldsymbol{p}_{\mathrm{Lda1}}$ is used to compensate for the effect due to addition of the cross-coupling technology to the overall system dynamics. The necessity of introducing this term will be shown in the following controller design process. Let $\boldsymbol{e}_{\mathrm{p}}$=$\boldsymbol{p}_{\mathrm{L}}$−$\boldsymbol{p}_{\mathrm{Ld}}$ denote the virtual control input discrepancy. Substituting Eq. (19) into Eq. (18) gives

$$\dot{V}_1 = \boldsymbol{r}^{\mathrm{T}}A\boldsymbol{e}_{\mathrm{p}} - \boldsymbol{r}^{\mathrm{T}}\boldsymbol{K}_{\mathrm{p}}\boldsymbol{r} + \boldsymbol{r}^{\mathrm{T}}(A\boldsymbol{p}_{\mathrm{Lda2}} + A\boldsymbol{p}_{\mathrm{Lds2}} - \boldsymbol{\varphi}_1^{\mathrm{T}}\tilde{\boldsymbol{\theta}}_1 + \tilde{\boldsymbol{f}}_0) - \boldsymbol{r}^{\mathrm{T}}\boldsymbol{K}_{\boldsymbol{\varsigma}}\boldsymbol{T}^{\mathrm{T}}\boldsymbol{\varsigma} + \boldsymbol{\varsigma}^{\mathrm{T}}\boldsymbol{K}_{\boldsymbol{\varsigma}}\dot{\boldsymbol{\varsigma}} + \left(\int_0^t \boldsymbol{T}^{\mathrm{T}}\boldsymbol{\varsigma}\mathrm{d}\omega\right)^{\mathrm{T}} \boldsymbol{\beta}\boldsymbol{\Lambda}\boldsymbol{K}_{\boldsymbol{\varsigma}}\boldsymbol{T}^{\mathrm{T}}\boldsymbol{\varsigma}. \tag{20}$$

Substituting Eq. (15) into the term $\boldsymbol{r}^{\mathrm{T}}\boldsymbol{K}_{\boldsymbol{\varsigma}}\boldsymbol{T}^{\mathrm{T}}\boldsymbol{\varsigma}$ in Eq. (20) leads to

$$\dot{V}_1 = \boldsymbol{r}^{\mathrm{T}}A\boldsymbol{e}_{\mathrm{p}} - \boldsymbol{r}^{\mathrm{T}}\boldsymbol{K}_{\mathrm{p}}\boldsymbol{r} + \boldsymbol{r}^{\mathrm{T}}(A\boldsymbol{p}_{\mathrm{Lda2}} + A\boldsymbol{p}_{\mathrm{Lds2}} - \boldsymbol{\varphi}_1^{\mathrm{T}}\tilde{\boldsymbol{\theta}}_1 + \tilde{\boldsymbol{f}}_0) - (\boldsymbol{T}^{\mathrm{T}}\boldsymbol{\varsigma})^{\mathrm{T}}\boldsymbol{\beta}^{\mathrm{T}}\boldsymbol{K}_{\boldsymbol{\varsigma}}(\boldsymbol{T}^{\mathrm{T}}\boldsymbol{\varsigma}) - \boldsymbol{\varsigma}^{\mathrm{T}}\boldsymbol{\Lambda}^{\mathrm{T}}\boldsymbol{K}_{\boldsymbol{\varsigma}}\boldsymbol{\varsigma}. \tag{21}$$

In practice, the uncertain nonlinearity $\tilde{\boldsymbol{f}}_0$ and the model uncertainties due to parameter estimation error $\tilde{\boldsymbol{\theta}}_1$ together can be categorized into a low frequency component $\boldsymbol{d}_{\mathrm{c1}}$ and a high frequency component $\boldsymbol{\Delta}_1(t)$, i.e.,

$$\boldsymbol{d}_{\mathrm{c1}} + \boldsymbol{\Delta}_1(t) = -\boldsymbol{\varphi}_1^{\mathrm{T}}\tilde{\boldsymbol{\theta}}_1 + \tilde{\boldsymbol{f}}_0. \tag{22}$$

As done in Meng *et al.* (2013), the low frequency component $\boldsymbol{d}_{\mathrm{c1}}$ can be compensated using $\boldsymbol{p}_{\mathrm{Lda2}}$ as follows:

$$\boldsymbol{p}_{\mathrm{Lda2}} = -\frac{1}{A}\hat{\boldsymbol{d}}_{\mathrm{c1}}, \tag{23}$$

where $\hat{\boldsymbol{d}}_{\mathrm{c1}}$ represents the estimate of $\boldsymbol{d}_{\mathrm{c1}}$ updated by

$$\dot{\hat{\boldsymbol{d}}}_{\mathrm{c1}} = \mathrm{Proj}_{\hat{\boldsymbol{d}}_{\mathrm{c1}}}(\boldsymbol{\gamma}_{\mathrm{c1}}\boldsymbol{r}) = \begin{cases} \boldsymbol{0}, & \|\hat{\boldsymbol{d}}_{\mathrm{c1}}(t)\| = d_{\mathrm{c1M}} \text{ and } \hat{\boldsymbol{d}}_{\mathrm{c1}}^{\mathrm{T}}(t)\boldsymbol{r} > 0, \\ \boldsymbol{\gamma}_{\mathrm{c1}}\boldsymbol{r}, & \text{else}, \end{cases} \tag{24}$$

with $\|\hat{\boldsymbol{d}}_{\mathrm{c1}}(0)\| \le d_{\mathrm{c1M}}$, where $\boldsymbol{\gamma}_{\mathrm{c1}}$=diag{$\gamma_{\mathrm{c11}}$, γ_{c12}} is the positive-definite diagonal adaptation rate matrix and d_{c1M}>0 is a preset bound. Such a projection type adaptation law guarantees $\|\hat{\boldsymbol{d}}_{\mathrm{c1}}(t)\| \le d_{\mathrm{c1M}}$ $\forall t$. Substituting Eqs. (22) and (23) into Eq. (21) gives

$$\dot{V}_1 = \boldsymbol{r}^{\mathrm{T}}A\boldsymbol{e}_{\mathrm{p}} - \boldsymbol{r}^{\mathrm{T}}\boldsymbol{K}_{\mathrm{p}}\boldsymbol{r} + \boldsymbol{r}^{\mathrm{T}}[A\boldsymbol{p}_{\mathrm{Lds2}} - \tilde{\boldsymbol{d}}_{\mathrm{c1}} + \boldsymbol{\Delta}_1(t)] - (\boldsymbol{T}^{\mathrm{T}}\boldsymbol{\varsigma})^{\mathrm{T}}\boldsymbol{\beta}^{\mathrm{T}}\boldsymbol{K}_{\boldsymbol{\varsigma}}(\boldsymbol{T}^{\mathrm{T}}\boldsymbol{\varsigma}) - \boldsymbol{\varsigma}^{\mathrm{T}}\boldsymbol{\Lambda}^{\mathrm{T}}\boldsymbol{K}_{\boldsymbol{\varsigma}}\boldsymbol{\varsigma} = \boldsymbol{r}^{\mathrm{T}}A\boldsymbol{e}_{\mathrm{p}} + \dot{V}_1\big|_{\boldsymbol{p}_{\mathrm{Ld}}}, \tag{25}$$

where $\tilde{\boldsymbol{d}}_{\mathrm{c1}} = \hat{\boldsymbol{d}}_{\mathrm{c1}} - \boldsymbol{d}_{\mathrm{c1}}$, $\dot{V}_1\big|_{\boldsymbol{p}_{\mathrm{Ld}}}$ is a short-hand notation used to represent $\dot{V}_1$ when $\boldsymbol{e}_{\mathrm{p}}$=$\boldsymbol{0}$. The robust feedback term $\boldsymbol{p}_{\mathrm{Lds2}}$ is chosen to satisfy the following condition:

$$\boldsymbol{r}^{\mathrm{T}}[A\boldsymbol{p}_{\mathrm{Lds2}} - \tilde{\boldsymbol{d}}_{\mathrm{c1}} + \boldsymbol{\Delta}_1(t)] \le \eta_1, \tag{26}$$

where η_1>0 is a design parameter. Since projection mapping will be used to condition the parameter estimation algorithm so that the parameter estimates are kept within the known bounded convex set $\bar{\Omega}_{\boldsymbol{\theta}_1}$ (the closure of the convex set $\Omega_{\boldsymbol{\theta}_1}$), by assumption, $-\tilde{\boldsymbol{d}}_{\mathrm{c1}} + \boldsymbol{\Delta}_1(t)$ is bounded with some known functions

$h_1(t)$. For example, $h_1(t)$ can be any bounding function satisfying

$$h_1(t) \geq d_{c1M} + \|\boldsymbol{\theta}_{1M}\|\|\boldsymbol{\varphi}_1\| + f_{i\max}, \tag{27}$$

where $\boldsymbol{\theta}_{1M}=\boldsymbol{\theta}_{1\max}-\boldsymbol{\theta}_{1\min}$. Therefore, $\boldsymbol{p}_{Lds2}$ can be chosen as

$$\boldsymbol{p}_{Lds2} = -\frac{1}{A}\frac{h_1^2(t)}{4\eta_1}\boldsymbol{r}. \tag{28}$$

Substituting Eq. (26) into Eq. (25) leads to

$$\begin{aligned}\dot{V}_1 \leq\ & \boldsymbol{r}^{\mathrm{T}} A\boldsymbol{e}_{\mathrm{p}} - \boldsymbol{r}^{\mathrm{T}}\boldsymbol{K}_{\mathrm{p}}\boldsymbol{r} - (\boldsymbol{T}^{\mathrm{T}}\boldsymbol{\varsigma})^{\mathrm{T}}\boldsymbol{\beta}^{\mathrm{T}}\boldsymbol{K}_{\boldsymbol{\varsigma}}(\boldsymbol{T}^{\mathrm{T}}\boldsymbol{\varsigma}) \\ & - \boldsymbol{\varsigma}^{\mathrm{T}}\boldsymbol{\Lambda}^{\mathrm{T}}\boldsymbol{K}_{\boldsymbol{\varsigma}}\boldsymbol{\varsigma} + \eta_1.\end{aligned} \tag{29}$$

It is thus concluded that $\dot{V}_1$ can be made negative semi-definite by choosing a large enough feedback gain matrix $\boldsymbol{K}_{\mathrm{p}}$ and/or a small enough controller parameter η_1 when $\boldsymbol{e}_{\mathrm{p}}=\boldsymbol{0}$. As a result, $\boldsymbol{r}$ and the synchronization error vector $\boldsymbol{\varsigma}$ are bounded. Furthermore, the coupled position error $\boldsymbol{E}$ and its derivative $\dot{\boldsymbol{E}}$ are bounded according to Eq. (15). With the fact that $\boldsymbol{\varsigma}$ is bounded, one can conclude that $\boldsymbol{e}$ is also bounded from Eq. (13). Now we have explicitly illustrated that the motion trajectory tracking error $\boldsymbol{e}$ will be bounded and the synchronization goal is achieved if we can make $\boldsymbol{e}_{\mathrm{p}}$ converge to zero or a small value.

3.1.2 Step 2

Differentiating $\boldsymbol{e}_{\mathrm{p}}$ and noting Eq. (5) yield

$$\dot{\boldsymbol{e}}_{\mathrm{p}} = \boldsymbol{q}_{\mathrm{L}} + \boldsymbol{F}_{\mathrm{p}} + \boldsymbol{\varphi}_2^{\mathrm{T}}\boldsymbol{\theta}_2 + \tilde{\boldsymbol{d}}_0 - \dot{\boldsymbol{p}}_{\mathrm{Ldc}} - \dot{\boldsymbol{p}}_{\mathrm{Ldu}}, \tag{30}$$

where

$$\dot{\boldsymbol{p}}_{\mathrm{Ldc}} = \frac{\partial \boldsymbol{p}_{\mathrm{Ld}}}{\partial \boldsymbol{x}}\dot{\boldsymbol{x}} + \frac{\partial \boldsymbol{p}_{\mathrm{Ld}}}{\partial \dot{\boldsymbol{x}}}\hat{\dot{\boldsymbol{x}}} + \frac{\partial \boldsymbol{p}_{\mathrm{Ld}}}{\partial \hat{\boldsymbol{\theta}}_1}\dot{\hat{\boldsymbol{\theta}}}_1 + \frac{\partial \boldsymbol{p}_{\mathrm{Ld}}}{\partial \hat{\boldsymbol{d}}_{c1}}\dot{\hat{\boldsymbol{d}}}_{c1} + \frac{\partial \boldsymbol{p}_{\mathrm{Ld}}}{\partial t}$$

represents the calculable part of $\dot{\boldsymbol{p}}_{\mathrm{Ld}}$ and can be used to design control functions, $\hat{\dot{\boldsymbol{x}}} = \boldsymbol{M}^{-1}(A\boldsymbol{p}_{\mathrm{L}} + \boldsymbol{\varphi}_1^{\mathrm{T}}\hat{\boldsymbol{\theta}}_1)$ is the vector of estimated acceleration, and $\dot{\boldsymbol{p}}_{\mathrm{Ldu}} = \frac{\partial \boldsymbol{p}_{\mathrm{Ld}}}{\partial \dot{\boldsymbol{x}}}\boldsymbol{M}^{-1}(-\boldsymbol{\varphi}_1^{\mathrm{T}}\tilde{\boldsymbol{\theta}}_1 + \tilde{\boldsymbol{f}}_0)$ is the incalculable part of $\dot{\boldsymbol{p}}_{\mathrm{Ld}}$ due to various uncertainties and has to be dealt with by certain robust feedback as in step 1. Consider $\boldsymbol{q}_{\mathrm{L}}$ as the virtual control input. Therefore, the next step is to synthesize a control function $\boldsymbol{q}_{\mathrm{Ld}}$ for $\boldsymbol{q}_{\mathrm{L}}$ such that $\boldsymbol{e}_{\mathrm{p}}$ converges to zero or a small value with a guaranteed transient performance.

Define a positive semi-definite function

$$V_2 = V_1 + \frac{1}{2}\boldsymbol{e}_{\mathrm{p}}^{\mathrm{T}}\boldsymbol{e}_{\mathrm{p}}. \tag{31}$$

Differentiating V_2 and noting Eqs. (25) and (30) lead to

$$\dot{V}_2 = \dot{V}_1\big|_{\boldsymbol{p}_{\mathrm{Ld}}} + \boldsymbol{e}_{\mathrm{p}}^{\mathrm{T}}(\boldsymbol{q}_{\mathrm{L}} + A\boldsymbol{r} + \boldsymbol{F}_{\mathrm{p}} + \boldsymbol{\varphi}_2^{\mathrm{T}}\boldsymbol{\theta}_2 + \tilde{\boldsymbol{d}}_0 - \dot{\boldsymbol{p}}_{\mathrm{Ldc}} - \dot{\boldsymbol{p}}_{\mathrm{Ldu}}). \tag{32}$$

Similar to Eq. (19), the following control law $\boldsymbol{q}_{\mathrm{Ld}}$ for $\boldsymbol{q}_{\mathrm{L}}$ is proposed:

$$\boldsymbol{q}_{\mathrm{Ld}} = \boldsymbol{q}_{\mathrm{Lda1}} + \boldsymbol{q}_{\mathrm{Lda2}} + \boldsymbol{q}_{\mathrm{Lds1}} + \boldsymbol{q}_{\mathrm{Lds2}}, \tag{33}$$

where

$$\boldsymbol{q}_{\mathrm{Lda1}} = -A\boldsymbol{r} - \boldsymbol{F}_{\mathrm{p}} - \boldsymbol{\varphi}_2^{\mathrm{T}}\hat{\boldsymbol{\theta}}_2 + \dot{\boldsymbol{p}}_{\mathrm{Ldc}},\ \ \boldsymbol{q}_{\mathrm{Lds1}} = -\boldsymbol{K}_{\mathrm{q}}\boldsymbol{e}_{\mathrm{p}}.$$

$\boldsymbol{q}_{\mathrm{Lda1}}$ is the usual model compensation with the physical parameter estimate $\hat{\boldsymbol{\theta}}_2$ updated using an online adaption algorithm to be detailed in Section 3.2, $\boldsymbol{q}_{\mathrm{Lda2}}$ is the fast dynamic compensation term to be synthesized later, $\boldsymbol{q}_{\mathrm{Lds1}}$ is a negative feedback of $\boldsymbol{e}_{\mathrm{p}}$ to stabilize the nominal system, in which $\boldsymbol{K}_{\mathrm{q}}=\mathrm{diag}\{K_{\mathrm{q}1}, K_{\mathrm{q}2}\}$ is the positive-definite diagonal control gain matrix, and $\boldsymbol{q}_{\mathrm{Lds2}}$ is synthesized later to dominate the model uncertainties. Substituting Eq. (33) into Eq. (32) gives

$$\dot{V}_2 = \dot{V}_1\big|_{\boldsymbol{p}_{\mathrm{Ld}}} - \boldsymbol{e}_{\mathrm{p}}^{\mathrm{T}}\boldsymbol{K}_{\mathrm{q}}\boldsymbol{e}_{\mathrm{p}} + \boldsymbol{e}_{\mathrm{p}}^{\mathrm{T}}(\boldsymbol{q}_{\mathrm{Lda2}} + \boldsymbol{q}_{\mathrm{Lds2}} - \boldsymbol{\varphi}_2^{\mathrm{T}}\tilde{\boldsymbol{\theta}}_2 + \tilde{\boldsymbol{d}}_0 - \dot{\boldsymbol{p}}_{\mathrm{Ldu}}). \tag{34}$$

Similar to Eq. (22), define a constant vector $\boldsymbol{d}_{c2}$ and a time-varying function vector $\boldsymbol{\Delta}_2(t)$ such that

$$\boldsymbol{d}_{c2} + \boldsymbol{\Delta}_2(t) = -\boldsymbol{\varphi}_2^{\mathrm{T}}\tilde{\boldsymbol{\theta}}_2 + \tilde{\boldsymbol{d}}_0 - \dot{\boldsymbol{p}}_{\mathrm{Ldu}}. \tag{35}$$

As in step 1, the fast dynamic compensation term $\boldsymbol{q}_{\mathrm{Lda2}}$ can be chosen as

$$\boldsymbol{q}_{\mathrm{Lda2}} = -\hat{\boldsymbol{d}}_{c2}, \tag{36}$$

where $\hat{\boldsymbol{d}}_{c2}$ represents the estimate of $\boldsymbol{d}_{c2}$ updated by

$$\dot{\hat{\boldsymbol{d}}}_{\mathrm{c2}} = \mathrm{Proj}_{\hat{\boldsymbol{d}}_{\mathrm{c2}}}(\boldsymbol{\gamma}_{\mathrm{c2}}\boldsymbol{e}_{\mathrm{p}}) = \begin{cases} \boldsymbol{0}, & \|\hat{\boldsymbol{d}}_{\mathrm{c2}}(t)\| = d_{\mathrm{c2M}} \text{ and } \hat{\boldsymbol{d}}_{\mathrm{c2}}^{\mathrm{T}}(t)\boldsymbol{e}_{\mathrm{p}} > 0, \\ \boldsymbol{\gamma}_{\mathrm{c2}}\boldsymbol{e}_{\mathrm{p}}, & \text{else}, \end{cases} \quad (37)$$

with $\|\hat{\boldsymbol{d}}_{\mathrm{c2}}(0)\| \le d_{\mathrm{c2M}}$, where $\boldsymbol{\gamma}_{\mathrm{c2}}=\mathrm{diag}\{\gamma_{\mathrm{c21}}, \gamma_{\mathrm{c22}}\}$ is the positive-definite diagonal adaptation rate matrix and $d_{\mathrm{c2M}}>0$ is a preset bound. Such a projection type adaptation law guarantees $\|\hat{\boldsymbol{d}}_{\mathrm{c2}}(t)\| \le d_{\mathrm{c2M}}$ $\forall t$. Substituting Eqs. (35) and (36) into Eq. (34) gives

$$\dot{V}_2 = \dot{V}_1\big|_{\boldsymbol{p}_{\mathrm{Ld}}} - \boldsymbol{e}_{\mathrm{p}}^{\mathrm{T}}\boldsymbol{K}_{\mathrm{q}}\boldsymbol{e}_{\mathrm{p}} + \boldsymbol{e}_{\mathrm{p}}^{\mathrm{T}}[\boldsymbol{q}_{\mathrm{Lds2}} - \tilde{\boldsymbol{d}}_{\mathrm{c2}} + \boldsymbol{\Delta}_2(t)]. \quad (38)$$

Similarly, $\boldsymbol{q}_{\mathrm{Lds2}}$ is chosen to satisfy the following condition:

$$\boldsymbol{e}_{\mathrm{p}}^{\mathrm{T}}[\boldsymbol{q}_{\mathrm{Lds2}} - \tilde{\boldsymbol{d}}_{\mathrm{c2}} + \boldsymbol{\Delta}_2(t)] \le \eta_2, \quad (39)$$

where $\eta_2>0$ is a design parameter. One example of $\boldsymbol{q}_{\mathrm{Lds2}}$ is given by

$$\boldsymbol{q}_{\mathrm{Lds2}} = -\frac{h_2^2(t)}{4\eta_2}\boldsymbol{e}_{\mathrm{p}}, \quad (40)$$

where $h_2(t)$ can be any bounding function satisfying

$$h_2(t) \ge \left\|\frac{\partial \boldsymbol{p}_{\mathrm{Ld}}}{\partial \dot{\boldsymbol{x}}}\boldsymbol{M}^{-1}\right\|(\|\boldsymbol{\theta}_{\mathrm{2M}}\|\|\boldsymbol{\varphi}_2\| + f_{\max}) + d_{\mathrm{c2M}} + \|\boldsymbol{\theta}_{\mathrm{2M}}\|\|\boldsymbol{\varphi}_2\| + d_{\max}, \quad (41)$$

where $\boldsymbol{\theta}_{\mathrm{2M}}=\boldsymbol{\theta}_{\mathrm{2max}}-\boldsymbol{\theta}_{\mathrm{2min}}$. Substituting Eq. (39) into Eq. (38) leads to

$$\dot{V}_2 \le -\boldsymbol{r}^{\mathrm{T}}\boldsymbol{K}_{\mathrm{p}}\boldsymbol{r} - \boldsymbol{e}_{\mathrm{p}}^{\mathrm{T}}\boldsymbol{K}_{\mathrm{q}}\boldsymbol{e}_{\mathrm{p}} - (\boldsymbol{T}^{\mathrm{T}}\boldsymbol{\varsigma})^{\mathrm{T}}\boldsymbol{\beta}^{\mathrm{T}}\boldsymbol{K}_{\boldsymbol{\varsigma}}(\boldsymbol{T}^{\mathrm{T}}\boldsymbol{\varsigma}) - \boldsymbol{\varsigma}^{\mathrm{T}}\boldsymbol{\Lambda}^{\mathrm{T}}\boldsymbol{K}_{\boldsymbol{\varsigma}}\boldsymbol{\varsigma} + \eta_1 + \eta_2. \quad (42)$$

Clearly, $\dot{V}_2$ can be made negative semi-definite and $\boldsymbol{e}_{\mathrm{p}}$ can be made converge to zero or a small value by increasing feedback gain vectors $\boldsymbol{K}_{\mathrm{p}}$, $\boldsymbol{K}_{\mathrm{q}}$ and/or decreasing controller parameters η_1, η_2.

3.1.3 Step 3

Once $\boldsymbol{q}_{\mathrm{Ld}}=[q_{\mathrm{Ld1}}, q_{\mathrm{Ld2}}]^{\mathrm{T}}$ is calculated, the desired effective valve orifice areas $A_1(u_1)$ and $A_2(u_2)$ of the two control valves can be calculated by

$$A_i(u_i) = \begin{cases} \dfrac{q_{\mathrm{Ld}i}}{\gamma RT_{\mathrm{s}}K_{\mathrm{q}}(p_{\mathrm{s}}, p_{ai}, T_{\mathrm{s}})/V_{ai} + \gamma RT_{\mathrm{b}i}K_{\mathrm{q}}(p_{\mathrm{b}i}, p_0, T_{\mathrm{b}i})/V_{\mathrm{b}i}}, & q_{\mathrm{Ld}i} \ge 0, \\ \dfrac{q_{\mathrm{Ld}i}}{-\gamma RT_{ai}K_{\mathrm{q}}(p_{ai}, p_0, T_{ai})/V_{ai} - \gamma RT_{\mathrm{s}}K_{\mathrm{q}}(p_{\mathrm{s}}, p_{\mathrm{b}i}, T_{\mathrm{s}})/V_{\mathrm{b}i}}, & q_{\mathrm{Ld}i} < 0, \end{cases} \quad (43)$$

where i=1, 2. Thus, the input signal $\boldsymbol{u}=[u_1, u_2]^{\mathrm{T}}$ for the proportional directional control valves can be obtained according to the relationship between the input signal and effective valve orifice area (Fig. 2).

3.2 Parameter estimation algorithm

In this subsection, online recursive least squares estimation (RLSE) of $\boldsymbol{\theta}_1$ and $\boldsymbol{\theta}_2$ will be developed for reducing parametric uncertainties. As mentioned in Section 3.1, the widely used projection mapping in adaptive control will be used to condition the RLSE algorithm so that the parameter estimates are kept within the known bounded convex sets $\Omega_{\boldsymbol{\theta}_1}$ and $\Omega_{\boldsymbol{\theta}_2}$. Otherwise, no bounded robust control terms $\boldsymbol{p}_{\mathrm{Lds2}}$ and $\boldsymbol{q}_{\mathrm{Lds2}}$ can be found to attenuate the unbounded model uncertainties in Eq. (26) and Eq. (39), respectively.

Assume the system is free of uncertain nonlinearities, i.e., $\tilde{\boldsymbol{f}}_0=\tilde{\boldsymbol{d}}_0=\boldsymbol{0}$ in Eqs. (3) and (5). Rewriting Eqs. (3) and (5), the following linear regression models can be constructed:

$$\boldsymbol{y}_1 = \boldsymbol{M}\ddot{\boldsymbol{x}} - A\boldsymbol{p}_{\mathrm{L}} = \boldsymbol{\varphi}_1^{\mathrm{T}}\boldsymbol{\theta}_1, \quad (44)$$

$$\boldsymbol{y}_2 = \dot{\boldsymbol{p}}_{\mathrm{L}} - \boldsymbol{q}_{\mathrm{L}} - \boldsymbol{F}_{\mathrm{p}} = \boldsymbol{\varphi}_2^{\mathrm{T}}\boldsymbol{\theta}_2. \quad (45)$$

Let $H_{\mathrm{f}}(\mathrm{s})$ be a stable LTI filter transfer function with a relative degree 3, e.g.,

$$H_{\mathrm{f}}(s) = \frac{\omega_{\mathrm{f}}^2}{(\tau_{\mathrm{f}}s+1)(s^2+2\xi\omega_{\mathrm{f}}s+\omega_{\mathrm{f}}^2)}, \quad (46)$$

where τ_{f}, ω_{f}, and ξ are filter parameters. Applying the filter to both sides of Eqs. (3) and (5), one obtains the filtered linear regression models:

$$\boldsymbol{y}_{1\mathrm{f}} = H_{\mathrm{f}}(\boldsymbol{M}\ddot{\boldsymbol{x}} - A\boldsymbol{p}_{\mathrm{L}}) = \boldsymbol{\varphi}_{1\mathrm{f}}^{\mathrm{T}}\boldsymbol{\theta}_1, \quad (47)$$

$$\boldsymbol{y}_{2\mathrm{f}} = H_{\mathrm{f}}(\dot{\boldsymbol{p}}_{\mathrm{L}} - \boldsymbol{q}_{\mathrm{L}} - \boldsymbol{F}_{\mathrm{p}}) = \boldsymbol{\varphi}_{2\mathrm{f}}^{\mathrm{T}}\boldsymbol{\theta}_2, \quad (48)$$

where $\boldsymbol{\varphi}_{1\mathrm{f}}^{\mathrm{T}}=\begin{bmatrix}\dot{x}_{1\mathrm{f}} & S_{\mathrm{f1f}}(\dot{x}_1) & 1_{\mathrm{f}} & 0 & 0 & 0\\ 0 & 0 & 0 & \dot{x}_{2\mathrm{f}} & S_{\mathrm{f2f}}(\dot{x}_2) & 1_{\mathrm{f}}\end{bmatrix}$ and $\boldsymbol{\varphi}_{2\mathrm{f}}^{\mathrm{T}}=\begin{bmatrix}1_{\mathrm{f}} & 0\\ 0 & 1_{\mathrm{f}}\end{bmatrix}$ are the filtered regressors, in which $\dot{x}_{1\mathrm{f}}$, $\dot{x}_{2\mathrm{f}}$, $S_{\mathrm{f1f}}(\dot{x}_1)$, $S_{\mathrm{f2f}}(\dot{x}_2)$, and 1_{f} represent the output of the filter for the input $\dot{x}_1$, $\dot{x}_2$, $S_{\mathrm{f1}}(\dot{x}_1)$, $S_{\mathrm{f2}}(\dot{x}_2)$, and 1, respectively. Defining the predicted output as $\hat{\boldsymbol{y}}_{i\mathrm{f}}=\boldsymbol{\varphi}_{i\mathrm{f}}^{\mathrm{T}}\hat{\boldsymbol{\theta}}_i$ leads to the following prediction error model:

$$\boldsymbol{\varepsilon}_i=\hat{\boldsymbol{y}}_{i\mathrm{f}}-\boldsymbol{y}_{i\mathrm{f}}=\boldsymbol{\varphi}_{i\mathrm{f}}^{\mathrm{T}}\tilde{\boldsymbol{\theta}}_i,\quad i=1,2. \tag{49}$$

To achieve a complete separation of estimator design and robust control law design, in addition to projection mapping, it is necessary to use the preset adaption rate limits for a controlled estimation process. Therefore, for each set of unknown parameter vectors, $\hat{\boldsymbol{\theta}}_i$ is updated using the following projection type adaption law with a preset adaption rate limit $\dot{\boldsymbol{\theta}}_{i\mathrm{M}}$:

$$\dot{\hat{\boldsymbol{\theta}}}_i=\mathrm{sat}_{\boldsymbol{\theta}_{i\mathrm{M}}}(\mathrm{Proj}_{\hat{\boldsymbol{\theta}}}(\boldsymbol{\Gamma}_i\boldsymbol{\tau}_i)),\quad i=1,2, \tag{50}$$

where $\boldsymbol{\tau}_i$ is the adaption function, $\boldsymbol{\Gamma}_i$ is the positive-definite symmetric adaption rate matrix, $\mathrm{Proj}_{\hat{\boldsymbol{\theta}}}(\boldsymbol{\Gamma}_i\boldsymbol{\tau}_i)$ is the standard projection mapping, and $\mathrm{sat}_{\boldsymbol{\theta}_{i\mathrm{M}}}(\bullet)$ is a saturation function defined by Eq. (52).

The standard projection mapping is

$$\mathrm{Proj}_{\hat{\boldsymbol{\theta}}}(\boldsymbol{\Gamma}_i\boldsymbol{\tau}_i)=\begin{cases}\boldsymbol{\Gamma}_i\boldsymbol{\tau}_i, & \hat{\boldsymbol{\theta}}_i\in\overset{\circ}{\Omega}_{\boldsymbol{\theta}_i}\ \text{or}\ \boldsymbol{n}_{\hat{\boldsymbol{\theta}}_i}^{\mathrm{T}}\boldsymbol{\Gamma}_i\boldsymbol{\tau}_i\le 0,\\ \left(1-\boldsymbol{\Gamma}_i\dfrac{\boldsymbol{n}_{\hat{\boldsymbol{\theta}}_i}\boldsymbol{n}_{\hat{\boldsymbol{\theta}}_i}^{\mathrm{T}}}{\boldsymbol{n}_{\hat{\boldsymbol{\theta}}_i}^{\mathrm{T}}\boldsymbol{\Gamma}_i\boldsymbol{n}_{\hat{\boldsymbol{\theta}}_i}}\right)\boldsymbol{\Gamma}_i\boldsymbol{\tau}_i, & \hat{\boldsymbol{\theta}}_i\in\partial\Omega_{\boldsymbol{\theta}_i}\ \text{or}\ \boldsymbol{n}_{\hat{\boldsymbol{\theta}}_i}^{\mathrm{T}}\boldsymbol{\Gamma}_i\boldsymbol{\tau}_i>0,\end{cases} \tag{51}$$

where $\overset{\circ}{\Omega}_{\boldsymbol{\theta}_i}$ and $\partial\Omega_{\boldsymbol{\theta}_i}$ denote the interior and the boundary of $\Omega_{\boldsymbol{\theta}_i}$, respectively, and $\boldsymbol{n}_{\hat{\boldsymbol{\theta}}_i}$ represents the outward unit normal vector at $\hat{\boldsymbol{\theta}}_i\in\partial\Omega_{\boldsymbol{\theta}_i}$.

The saturation function is defined as

$$\mathrm{sat}_{\boldsymbol{\theta}_{i\mathrm{M}}}(\bullet)=s_0\bullet,\quad s_0=\begin{cases}1, & \|\bullet\|\le\left\|\dot{\boldsymbol{\theta}}_{i\mathrm{M}}\right\|,\\ \dfrac{\left\|\dot{\boldsymbol{\theta}}_{i\mathrm{M}}\right\|}{\|\bullet\|}, & \|\bullet\|>\left\|\dot{\boldsymbol{\theta}}_{i\mathrm{M}}\right\|,\end{cases} \tag{52}$$

where $\dot{\boldsymbol{\theta}}_{i\mathrm{M}}$ is the preset adaption rate limit. The adaption rate matrix $\boldsymbol{\Gamma}_i$ is given by

$$\dot{\boldsymbol{\Gamma}}_i=\begin{cases}\alpha_i\boldsymbol{\Gamma}_i-\dfrac{\boldsymbol{\Gamma}_i\boldsymbol{\varphi}_{i\mathrm{f}}\boldsymbol{\varphi}_{i\mathrm{f}}^{\mathrm{T}}\boldsymbol{\Gamma}_i}{1+\nu_i\boldsymbol{\varphi}_{i\mathrm{f}}^{\mathrm{T}}\boldsymbol{\Gamma}_i\boldsymbol{\varphi}_{i\mathrm{f}}},\\ \quad\lambda_{\max}(\boldsymbol{\Gamma}_i(t))\le\rho_{i\mathrm{M}}\ \text{and}\ \left\|\mathrm{Proj}_{\hat{\boldsymbol{\theta}}}(\boldsymbol{\Gamma}_i\boldsymbol{\tau}_i)\right\|\le\left\|\dot{\boldsymbol{\theta}}_{i\mathrm{M}}\right\|,\\ \boldsymbol{0},\\ \quad\text{otherwise},\end{cases} \tag{53}$$

where $\alpha_i\ge 0$ is the forgetting factor, $\nu_i\ge 0$ is the normalizing factor with $\nu_i=0$ leading to the unnormalized algorithm, $\rho_{i\mathrm{M}}$ is the preset upper bound for $\|\boldsymbol{\Gamma}_i(t)\|$ which guarantees $\boldsymbol{\Gamma}_i(t)\le\rho_{i\mathrm{M}}\boldsymbol{I}\ \forall t$, and the adaption function $\boldsymbol{\tau}_i$ is given by

$$\boldsymbol{\tau}_i=\frac{1}{1+\nu_i\boldsymbol{\varphi}_{i\mathrm{f}}^{\mathrm{T}}\boldsymbol{\Gamma}_i\boldsymbol{\varphi}_{i\mathrm{f}}}\boldsymbol{\varphi}_{i\mathrm{f}}\varepsilon_i. \tag{54}$$

4 Experimental results

Experiments were performed on the dual-cylinder pneumatic system as shown in Fig. 1 to verify the proposed adaptive robust synchronization controller. Fig. 3 is the picture of the experimental setup. Each rodless cylinder (FESTO DGC-25-500-G-PPV-A) was controlled by a proportional directional control valve (FESTO MPYE-5-1/8-HF-010B). The pressure sensors (FESTO SDET-22T-D10-G14-I-M12) were used to measure the chamber pressures of each rodless cylinder and the tank pressure. Position and velocity information of the cylinder movement was obtained by the magnetostrictive linear position sensor (MTS RPS0500MD601V810050). Two single-rod cylinders, controlled by pressure control valves, were employed to produce a load force or simulate a disturbance on the rodless cylinder. The control algorithms were implemented using a dSPACE DS1103 controller board, while an industrial computer was used as the user interface. The controller executed programs at a sampling period of 1 ms.

Fig. 3 Picture of the experimental setup

The system physical parameters were m_1=m_2=2.6 kg, A_1=A_2=4.908×10^{-4} m^2, L_1=L_2=0.5 m, V_{1a0}=V_{2a0}=2.5×10^{-5} m^3, V_{1b0}=V_{2b0}=5×10^{-5} m^3, R=287 N·m/(kg·K), γ=1.4, T_s=300 K, p_s=7×10^5 Pa, p_0=1×10^5 Pa, h=60 W/(m^2·K). The nominal values of the uncertain parameters were set as θ_{11}=100 N·s/m, θ_{12}=80 N, θ_{13}=0 N, θ_{14}=100 N·s/m, θ_{15}=80 N, θ_{16}=0 N, θ_{21}=θ_{22}=0 Pa/s. The bounds of the parametric variations were chosen as $\boldsymbol{\theta}_{1\min}$=[0, 0, −100, 0, 0, −100]$^{\mathrm{T}}$, $\boldsymbol{\theta}_{2\min}$=[−100, −100]$^{\mathrm{T}}$, $\boldsymbol{\theta}_{1\max}$=[300, 250, 100, 300, 250, 100]$^{\mathrm{T}}$ and $\boldsymbol{\theta}_{2\max}$=[100, 100]$^{\mathrm{T}}$.

Using a trial-and-error procedure, the controller parameters adopted were $\boldsymbol{\beta}$=diag{0.3, 0.3}, $\boldsymbol{\Lambda}$=diag{100, 100}, $\boldsymbol{K}_\varsigma$=diag{45, 45}, $\boldsymbol{K}_\mathrm{p}$=diag{30, 40}, $h_1(t)$=100, η_1=4, $\boldsymbol{\gamma}_{\mathrm{c}1}$=diag{150, 150}, $d_{\mathrm{c}1\mathrm{M}}$=10, $\boldsymbol{K}_\mathrm{q}$=diag{400, 400}, $h_2(t)$=400, η_2=10, $\boldsymbol{\gamma}_{\mathrm{c}2}$=diag{10, 10}, $d_{\mathrm{c}2\mathrm{M}}$=10. The initial values of the adaption rate matrices were set as $\boldsymbol{\Gamma}_1$=diag{100, 100, 100, 100, 100, 100}, $\boldsymbol{\Gamma}_2$=diag{10, 10}. Other parameters in the parameter estimation algorithm were α_1=α_2=0.1, v_1=v_2=0.1, $\dot{\boldsymbol{\theta}}_{1\mathrm{M}}=[10, 10, 10, 10, 10, 10]^{\mathrm{T}}$, $\dot{\boldsymbol{\theta}}_{2\mathrm{M}}=[5, 5]^{\mathrm{T}}$, $\rho_{1\mathrm{M}}$=1000, $\rho_{2\mathrm{M}}$=100. The filter parameters were chosen as τ_f=50, ω_f=100, and ξ=1. The smooth function vector can be chosen as $\boldsymbol{S}_\mathrm{f}(\dot{\boldsymbol{x}})=\left[\frac{2}{\pi}\arctan(1000\dot{x}_1),\ \frac{2}{\pi}\arctan(1000\dot{x}_2)\right]^{\mathrm{T}}$.

The controller was first tested for tracking sinusoidal trajectories with different frequencies. Fig. 4 shows the synchronization error and the tracking errors of two cylinders for a sinusoidal trajectory motion with a frequency of 0.25 Hz and amplitude of 0.125 m. The average tracking errors of two cylinders in terms of L_2 norm were $L_2[e_1]$=0.72 mm and $L_2[e_2]$=0.68 mm, and the maximum absolute tracking errors were 1.31 mm and 1.40 mm. The average synchronization error in terms of L_2 norm was $L_2[\varsigma_1]$=$L_2[\varsigma_2]$=0.48 mm and the maximum absolute synchronization error was 1.05 mm. The proposed controller can effectively reduce the synchronization error between two cylinders (Jang *et al.*, 2004; Shibata *et al.*, 2006), while guaranteeing a prescribed motion trajectory tracking transient performance and final tracking accuracy. Fig. 5 shows the history of online parameter estimates. The estimates of parameters all converged quickly and stayed close to some constant values.

For tracking a faster sinusoidal trajectory (amplitude 0.125 m and frequency 0.5 Hz), the synchronization error and the tracking errors of two cylinders are shown in Fig. 6. The history of online parameter estimates is shown in Fig. 7. The average tracking errors of two cylinders in terms of L_2 norm were $L_2[e_1]$=0.93 mm and $L_2[e_2]$=0.95 mm, and the maximum absolute tracking errors were 2.19 mm and 2.25 mm. The average synchronization errors in terms of L_2 norm were $L_2[\varsigma_1]$=$L_2[\varsigma_2]$=0.49 mm and the maximum absolute synchronization error was 1.45 mm.

For tracking a smooth step trajectory, which has a maximum velocity of $\dot{x}_{d\max}$=0.3 m/s and a maximum acceleration of $\ddot{x}_{d\max}$=0.75π m/s^2, Fig. 8 shows the steady-state response of the system. The maximum absolute synchronization error was about 0.92 mm, and the final steady-state synchronization error was below 0.05 mm.

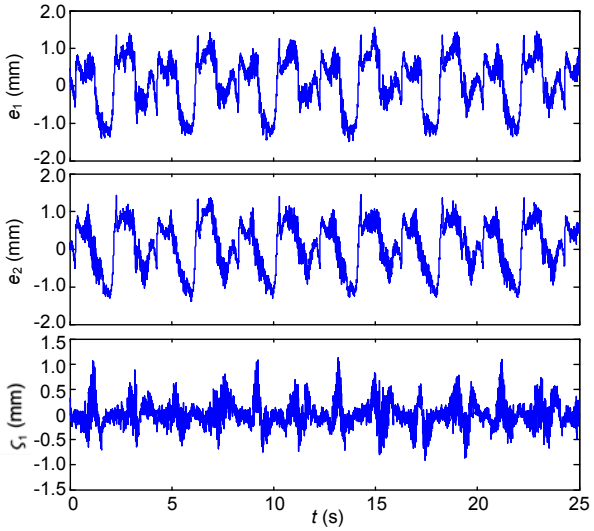

Fig. 4 Tracking errors and synchronization error for a 0.25 Hz sinusoidal trajectory

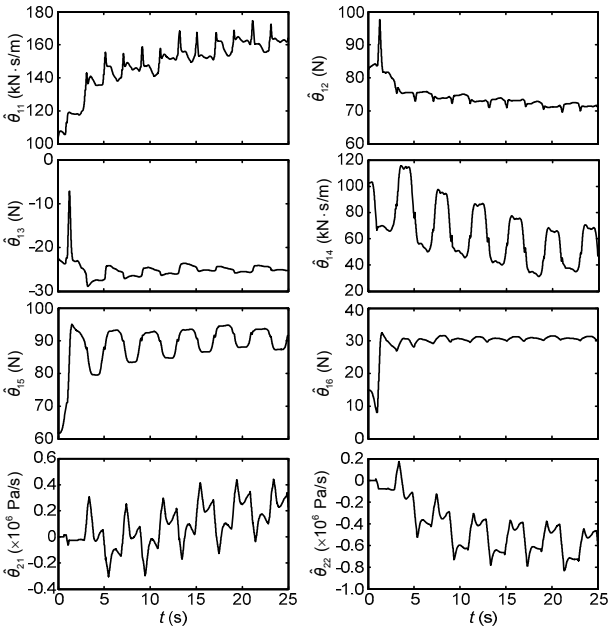

Fig. 5 Parameter estimation for a 0.25 Hz sinusoidal trajectory

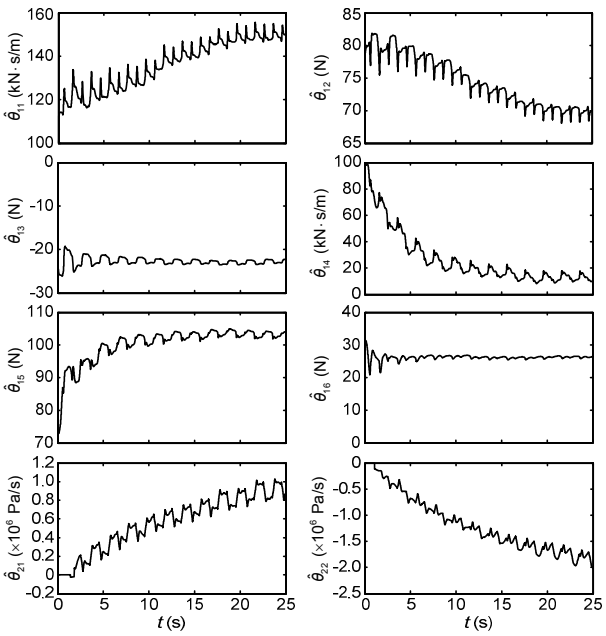

Fig. 7 Parameter estimation for a 0.5 Hz sinusoidal trajectory

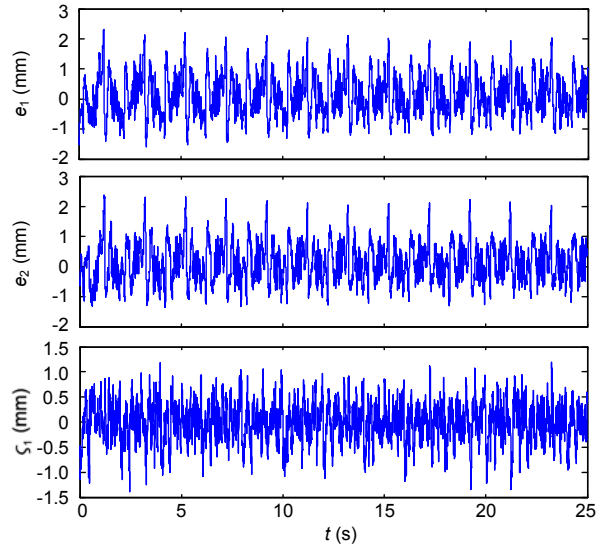

Fig. 6 Tracking errors and synchronization error for a 0.5 Hz sinusoidal trajectory

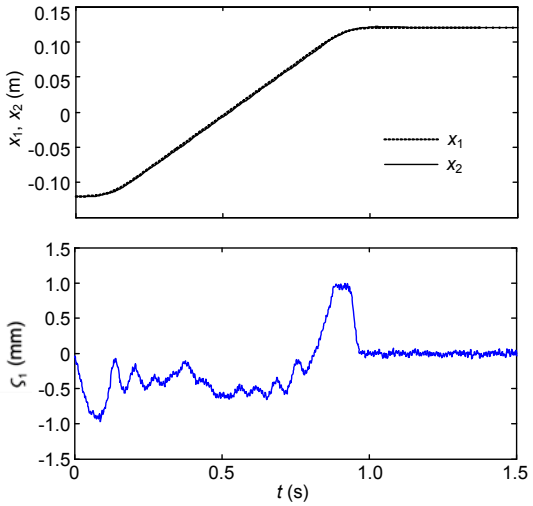

Fig. 8 Steady-state tracking response of the smooth step trajectory

To further test the achievable control performance of the proposed synchronization controller, the trajectory x_d=0.05sin(1.25πt)+0.05sin(πt)+0.05sin(0.5πt) was considered. Fig. 9 shows the synchronization error and the tracking errors of the system. As can be seen, the average tracking errors of two cylinders in terms of L_2 norm were $L_2[e_1]$=1.22 mm and $L_2[e_2]$=1.24 mm, and the maximum absolute tracking errors were 2.79 mm and 2.68 mm. The average synchronization errors in terms of L_2 norm were $L_2[\varsigma_1]$=$L_2[\varsigma_2]$=0.52 mm and the maximum absolute steady-state synchronization error was about 1.44 mm. The process of parameter estimation is shown in Fig. 10.

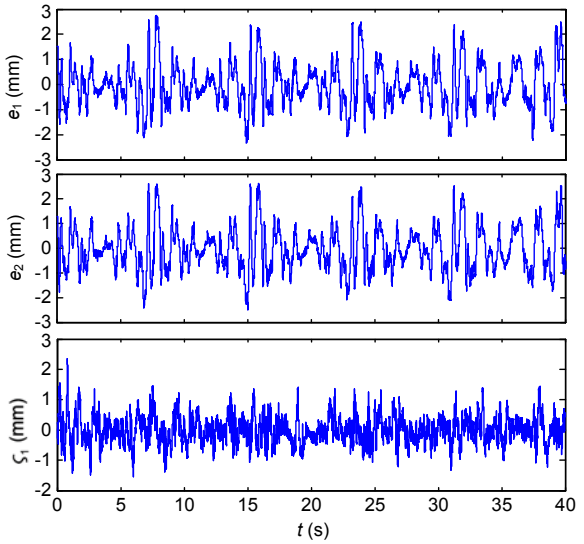

Fig. 9 Tracking errors and synchronization error for the periodic trajectory (period=8 s)

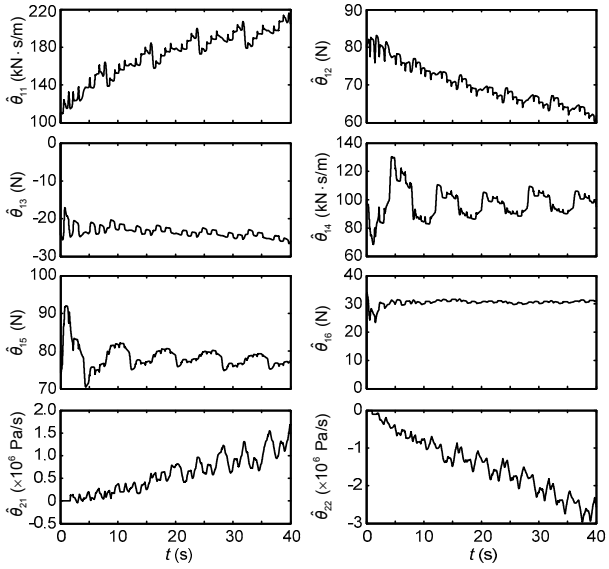

Fig. 10 Parameter estimation for the periodic trajectory (period=8 s)

A large external load force was added to cylinder 1 at t=7.5 s and removed at t=12.5 s to test the performance robustness of the proposed synchronization controller to sudden disturbance. Fig. 11 shows the steady-state synchronization error of the system in this situation for the trajectory x_d=0.125sin(πt). As can be seen, the added disturbance did not affect the control performance much except the transient spikes when sudden changes of the disturbance occurred.

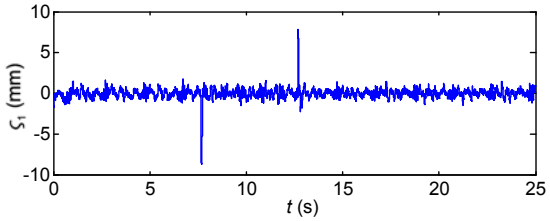

Fig. 11 Steady-state synchronization error for 0.5 Hz sinusoidal trajectory motion with disturbance

5 Conclusions

This paper presents an adaptive robust synchronization control strategy for two pneumatic cylinders. The cross-coupling technology is incorporated into the DIARC architecture and the proposed controller is synthesized with the feedback of the so-called coupled position error, which is a combination of the trajectory tracking errors of two cylinders and the position synchronization error between them. The adaptive robust synchronization controller employs an online RLSE algorithm to obtain accurate estimates of model parameters for reducing the extent of parametric uncertainties, and uses a robust control law to attenuate the effects of parameter estimation errors, unmodeled dynamics, and disturbances. Due to the use of projection mapping, the robust control law and the parameter adaption algorithm are designed separately. Since the system model uncertainties are unmatched, the recursive backstepping technology is adopted to design the robust control law. Theoretically, asymptotic convergence to zero is achieved for both position synchronization and trajectory tracking errors. Extensive experimental results illustrate the effectiveness of the proposed controller and its performance robustness to sudden disturbances.

References

Carneiro, J.F., de Almeida, F.G., 2006. Reduced-order thermodynamic models for servo-pneumatic actuator chambers. *Proc. Inst. Mech. Eng. Part I: J. Syst. Contr. Eng.*, **220**(4): 301-314. [doi:10.1243/09596518JSCE203]

Chen, C., Liu, L., Cheng, C., *et al.*, 2008. Fuzzy controller design for synchronous motion in a dual-cylinder electrohydraulic system. *Contr. Eng. Pract.*, **16**(6):658-673. [doi:10.1016/j.conengprac.2007.08.005]

Chen, C.Y., 2007. Synchronous motion of two-cylinder electrohydraulic system with unbalanced loading and

uncertainties. *Proc. Inst. Mech. Eng. Part I: J. Syst. Contr. Eng.*, **221**(7):937-955. [doi:10.1243/09596518JSCE372]

Hsieh, M., Tung, C., Yao, W., *et al.*, 2007. Servo design of a vertical axis drive using dual linear motors for high speed electric discharge machining. *Int. J. Mach. Tools Manuf.*, **47**(3-4):546-554. [doi:10.1016/j.ijmachtools.2006.05.011]

Jang, J.S., Kim, Y.B., Lee, I.Y., *et al.*, 2004. Design of a synchronous position controller with a pneumatic cylinder driving system. SICE Annual Conf., p.2943-2947.

Koren, Y., 1980. Cross-coupled biaxial computer controls for manufacturing systems. *J. Dynam. Syst. Meas. Contr.*, **102**(4):265-272. [doi:10.1115/1.3149612]

Meng, D., Tao, G., Chen, J., *et al.*, 2011. Modeling of a pneumatic system for high-accuracy position control. Proc. Int. Conf. on Fluid Power and Mechatronics, p.505-510. [doi:10.1109/FPM.2011.6045817]

Meng, D., Tao, G., Zhu, X., 2013. Integrated direct/indirect adaptive robust motion trajectory tracking control of pneumatic cylinders. *Int. J. Contr.*, **86**(9):1620-1633. [doi:10.1080/00207179.2013.792002]

Shan, J., Liu, H., Nowotny, S., 2005. Synchronized trajectory-tracking control multiple 3-DOF experimental helicopters. *IEE Proc.-Contr. Theory Appl.*, **152**(6):683-692. [doi:10.1049/ip-cta:20050008]

Shibata, S., Yamamoto, T., Jindai, M., 2006. A synchronous mutual position control for vertical pneumatic servo system. *JSME Int. J. Ser. C*, **49**(1):197-204. [doi:10.1299/jsmec.49.197]

Su, Y., Sun, D., Ren, L., *et al.*, 2006. Integration of saturated PI synchronous control and PD feedback for control of parallel manipulators. *IEEE Trans. Robot.*, **22**(1):202-207. [doi:10.1109/TRO.2005.858852]

Sun, D., 2003. Position synchronization of multiple motion axis with adaptive coupling control. *Automatica*, **39**(6):997-1005. [doi:10.1016/S0005-1098(03)00037-2]

Sun, D., Mills, K., 2002. Adaptive synchronized control of coordination of multi-robot assembly tasks. *IEEE Trans. Robot. Autom.*, **18**(4):498-510. [doi:10.1109/TRA.2002.802229]

Sun, D., Lu, R., Mills, J.K., *et al.*, 2006. Synchronous tracking control of parallel manipulators using cross-coupling approach. *Int. J. Robot. Res.*, **25**(11):1137-1147. [doi:10.1177/0278364906072037]

Sun, D., Shao, X., Feng, G., 2007. A model-free cross-coupled control for position synchronization of multi-axis motions: theory and experiments. *IEEE Trans. Contr. Syst. Technol.*, **15**(2):306-314. [doi:10.1109/TCST.2006.883201]

Sun, D., Wang, C., Feng, G., 2009. A synchronization approach to trajectory tracking of multiple mobile robots while maintaining time-varying formations. *IEEE Trans. Robot.*, **25**(5):1074-1086. [doi:10.1109/TRO.2009.2027384]

Xiao, Y., Zhu, K., 2006. Optimal synchronization control of high-performance motion systems. *IEEE Trans. Ind. Electron.*, **53**(4):1160-1169. [doi:10.1109/TIE.2006.878317]

Xiao, Y., Zhu, K., Liaw, H., 2005. Generalized synchronization control of multi-axis motion systems. *Contr. Eng. Pract.*, **13**(7):809-819. [doi:10.1016/j.conengprac.2004.09.005]

Zhu, X., Cao, J., Tao, G., *et al.*, 2009. Synchronization strategy research of pneumatic servo system based on separate control of meter-in and meter-out. IEEE/ASME Int. Conf. on Advanced Intelligent Mechatronics, p.24-29. [doi:10.1109/AIM.2009.5230043]